<Supporting Information>

Graphene quantum dots as supramolecular linkers in metal organic framework for constructing metal atom electrocatalysts

Yujie Song,[a,b] Jiajie Li,[a] Yaqi Zhang,[a] Jiali Lou,[a] Yuanyuan Cui,[d] Hongwu Chen,[b,c] Chao Lin,[b,c] Xiaopeng Li,[b,c] Huilin Fan,[*c] Xiaokai Song[*a]

[a] Institute of Advanced Functional Materials for Energy, School of Chemistry and Chemical Engineering, Jiangsu University of Technology, Changzhou 213001, China

[b] State Key Laboratory for Modification of Chemical Fibers and Polymer, Materials & College of Materials Science and Engineering, Donghua University, Shanghai 201620, China

[c] School of New Energy, Ningbo University of Technology, Ningbo 315336, China.

[d] Shimadzu (China) Co, LTD, Shanghai 213164, China.

E-mail: xksong@jsut.edu.cn.

1. Experimental Procedures

1.1 Chemicals and materials

2-methylimidazole (98%) and Nafion (5 wt. % in lower aliphatic alcohols and water, contains 15-20% water; Nafion 1100EW) were purchased from Energy Chemical Co., Ltd. and Sigma-Aldrich, respectively. Other reagents and solvents were purchased from Sinopharm Co. Ltd. and used without further purification. Deionized (DI) water with resistivity higher than 18 MΩ cm^{-1} was used during the experiments.

1.2 Preparation of N-GQDs

The synthesis of N-GQDs was based on a reported procedure with small modifications. Typically, citric acid (0.21 g, 1 mmol) and urea (0.18 g, 3 mmol) were dissolved into 5 ml deionized (DI) water, and stirred to form a clear solution. Then the solution was transfered into a 50 ml Teflon lined stainless autoclave. The sealed autoclave was heated to 160 °C in an electric oven and kept for additional 4 hours. The product was collected by adding ethanol into the solution and centrifuged at 5000 rpm for 5 min, and finally dried in vacuum at 60 °C overnight prior to use.

1.3 Preparation of N-GQDs@ZIF-67-*n*

The synthesis of N-GQDs@ZIF-67-0 (ZIF-67) was based on a reported procedure with modifications.0 Typically, 2-methylimidazole (8.250 g, 0.1 mol) was dissolved in 120 mL of water; then $Co(NO_3)_2 \cdot 6H_2O$ (0.625 g, 2.15 mmol) in 18 mL of water was added into above solution under vigorous stirring for 12 min at 60 °C. Subsequently, the resulting mixture was aged without stirring for 24 h at room temperature. The resulting purple precipitates were collected by centrifugation, washed with water and methanol in sequence for at least three times, and finally dried in vacuum at 60 °C overnight prior to use. N-GQDs@ZIF-67-50 was prepared using a similar procedure of ZIF-67. Typically, a solid mixture of 2-methylimidazole (8.250 g, 0.1 mol) and N-GQDs (50.0 mg) were dissolved in 120 mL of water; then $Co(NO_3)_2 \cdot 6H_2O$ (0.625 g, 2.15 mmol) in 18 mL of water was added into above solution

under vigorous stirring for 12 min at 60 °C. Subsequently, the resulting mixture was aged without stirring for 24 h at room temperature. The resulting violet precipitates were collected by centrifugation, washed with water and methanol in sequence for at least three times, and finally dried in vacuum at 60 °C overnight prior to use. The preparation of deep blue N-GQDs@ZIF-67-150 was performed by a similar procedure of N-GQDs@ZIF-67-50 with different amount of N-GQDs, 150 mg for N-GQDs@ZIF-67-150.

1.4 Preparation of Co-NGC-*n* from N-GQDs@ZIF-67-*n*.

The 500 mg of activated Co-N-GQDs@ZIF-67-*n* powder was heated to 900 °C at a heating rate of 5 °C min^{-1} and carbonized at 900 °C for 2 h under flowing N_2 atmosphere, and cooled to room temperature naturally to obtain porous carbon materials. Then the inactive and unstable Co species in product were removed as far as possible by 1.0 M HCl aqueous solution washing at room temperature for 3 h for twice, and followed by washing thoroughly with plenty of water to yield Co-NGC-*n* catalysts. Finally, the products were dried in vacuum at 60 °C overnight prior to use.

1.5 Materials characterization

The morphology of the samples was characterized using a Hitachi SU-8000 field-emission scanning electron microscope (SEM) at an accelerating voltage of 5 kV. Transmission electron microscope (TEM) and elemental mapping analysis were measured by a JEM-2100 operated at 200 kV. Powder X-ray diffraction (PXRD) patterns were recorded in a PANalytical diffractometer Model PW3040/60 X'pert PRO using monochromated Cu Kα radiation (40 kV, 40 mA) at a scanning rate of 2° min^{-1}. Nitrogen sorption measurement was conducted using a Micromeritics ASAP 2020 system at 77 K. The surface areas of N-GQDs@ZIF-67-*n* were estimated based on the Brunauer−Emmett−Teller (BET) model and Langmuir model, respectively, by using the adsorption branch data in the relative pressure (P/P_0) range of 0.01−0.1. The surface areas of Co-NGC-*n* were obtained based on the BET model by using the data of adsorption branches in the relative pressure (P/P_0) range of 0.05−0.5. The total pore volumes and pore-size distributions were calculated from the adsorption branches of isotherms based on the density functional theory (DFT) method. X-ray photoelectron spectroscopy (XPS) spectra were

measured at room temperature using a PHI Quantera SXM (ULVAC-PHI) instrument with an Al Kα X-ray source. The region of survey spectra is 0 to 1400 eV and the region of high-resolution N 1s spectra is 392 to 412 eV. The percentage of N was calculated from the XPS survey spectrum by using N 1s peak. Raman scattering spectra were recorded with a Renishaw System 2000 spectrometer using the 514.5 nm line of Ar^+ for excitation.

1.6 Electrochemical measurements

The ORR measurements were performed in a typical three electrode system in a aqueous 0.1 M KOH electrolyte constantly purged with high-purity oxygen. An Ag/AgCl (3M KCl) electrode and a platinum wire of high purity were used as reference and counter electrode, respectively. The RDE electrode with a diameter of ϕ 3 mm was used as the substrate for the working electrode. The rotating speed of RDE was controlled from 400 to 2025 rpm. The catalyst (5 mg) was dispersed in a mixed solution of 0.96 mL of ethanol and 0.04 mL of 5 wt% Nafion solution, and then subjected to ultrasonication. The catalyst ink (8 μL) was dropped on the RDE electrode and then dried in the air. Cyclic voltammetry (CV) measurements were conducted at a scan rate of 50 mV s^{-1} and a rotation rate of 1600 rpm. To eliminate the influence of background current, the linear scan voltammetry (LSV) measurements were recorded at a scan rate of 1 mV s^{-1}. The EIS test was carried out from 10^6 Hz to 10^{-2} Hz and recorded at OCP with an amplitude of 10 mV. The tolerance of the electrocatalysts to methanol poisoning was evaluated by injecting 5 mL of 3 M methanol into the electrolyte (150 mL) during the chronoamperometric measurements. For comparison, Pt/C (20 wt% platinum, JM) was conducted on the same electrochemical tests. For the ORR at a RDE, the electron transfer numbers can be calculated with Koutecky–Levich equation:

$$\frac{1}{j} = \frac{1}{j_L} + \frac{1}{j_K} = \frac{1}{B\omega^{1/2}} + \frac{1}{nFkC_o} \quad (1)$$

$$B = 0.62nF D_o^{2/3} \nu^{-1/6} C_o \quad (2)$$

where j is the measured current density; j_K and j_L are the kinetic and diffusion-limiting current densities, respectively; ω is the angular velocity of the disk (= 2πN, N is the linear rotation speed); n represents the overall number of electrons transferred in oxygen reduction; F is the Faraday constant (F = 96485 C mol^{-1}); C_o is the bulk concentration of O_2 (1.2×10^{-6} mol cm^{-3}); D_o is the diffusion coefficient of O_2 in 0.1 M

KOH electrolyte (1.9×10^{-5} cm^2 s^{-1}); v is the kinematics viscosity for electrolyte, and k is the electron-transferred rate constant.

To obtain the electron transfer number (n) and hydrogen peroxide yield (% H_2O_2), a rotating ring disk electrode (RRDE) electrode (diameter: ϕ 4 mm) served as working electrode. The catalyst ink (12 μL) was dropped on the RRDE electrode and then dried in the air. The H_2O_2 yield (% H_2O_2) and electron transfer number (n) were calculated as the following equations:

$$\%H_2O_2 = 200 \times \frac{I_R/N}{I_D + I_R/N} \tag{3}$$

$$n = \frac{4}{1 + \frac{I_R}{I_D} \times N} \tag{4}$$

Where I_D and I_R are disk and ring currents, respectively, and N is the collection efficiency of the ring electrode.

The ion diffusion coefficient is obtained according to the following:

$$D_{OH^-} = \frac{R^2T^2}{2A^2n^4F^4C^2\sigma^2} \tag{5}$$

where R is the gas constant (8.314 J K^{-1} mol^{-1}), T is the room temperature (298 K), A is the the surface area of the electrode used for testing (0.19625 cm^2), n is the number of transferred electrons (4), F is the Faraday constant (96485 C mol^{-1}), C is the concentration of OH^- (0.1 mmol cm^{-3}). According to $Z' = R_s + R_{ct} + \sigma\omega^{-1/2}$, it can be concluded that σ is the slope of the plot of Z'.

1.7 Zinc air batteries (ZABs) measurement

1.7.1 Liquid ZABs

Liquid ZABs were assembled in a typical two electrode configuration, in which a metallic zinc foil of purity ~99.9% and an air electrode were used as anode and cathode, respectively. The air electrode used

a carbon paper-based gas diffusion layer (TORAY-YLS 30T). The catalyst ink was drop casted onto the gas diffusion layer and dried by a hot air gun (temperature set at 80 °C). The catalyst loading was controlled to 1.0 mg cm^{-2}. The electrolyte was aqueous 6 M KOH with 0.2 M zinc acetate, which was constantly purged with pure oxygen at a rate of 40 mL min^{-1}. Prior to performance tests, the electrolyte was also purged with oxygen for 30 min in order to saturate electrolyte with oxygen. The open circuit voltage, discharging and charging polarization curves were recorded using the CHI760E electrochemical workstation. Rate performance of the assembled ZABs were evaluated by recording voltage profiles during galvanostatic discharge at various current densities from 5 to 30 mA cm^{-2}. The constant current discharge-charge cycle curves and specific capacity of the batteries were carried out at room temperature using a battery test system (Land 3001A). The ZABs were discharged for 150 second and charged for 150 second at a current density of 10 mA cm^{-2} in each galvanostatic cycle. The specific capacity and energy density were calculated according to the following equations:

$$Specific\ capacity\ (mAh{\cdot}g^{-1}) = I \times t / w_{Zn} \tag{6}$$

where I is the applied current (A), t is the serving time (s), V is the average discharge voltage (V), and w_{Zn} is the weight of zinc consumed (g).

1.7.2 Flexible ZABs

Flexible solid-state ZAB is consisted of air electrode, polyacrylic acid (PAA) film and zinc foil, which were served as air electrode, solid electrolyte and anode, respectively. The air electrode consists of a piece of nickel foam (NF) on the air-facing side as the current collector, a gas diffusion layer (GDL) in the middle, and a carbon cloth layer coated with catalyst (catalyst loading of 1.0 mg cm^{-2}) on the electrolyte-facing side. To prepare PAA gel electrolyte: 1 g of *N, N*-methylene diacrylamide as a cross-linker and 5 g of acrylic acid were quickly poured into 20 mL of DI water containing 18 g of KOH under continuous stirring, followed by dissolving 1.5 g of zinc acetate. After stirring for 2 h, $K_2S_2O_8$ aqueous solution (0.12 g dissolved in 20 mL of DI water) as the initiator was added to the aforementioned solution in the square mold and then shaken vigorously to form the PAA gel. The polarization curves were recorded via linear sweep voltammetry (LSV) at room temperature on a CHI 760E electrochemical working station. Both the current density and power density were normalized to the effective surface area of the air electrode. The ZABs were discharged for 150 second and charged for 150 second at a current density of 1 mA cm^{-2} in

each galvanostatic cycle.

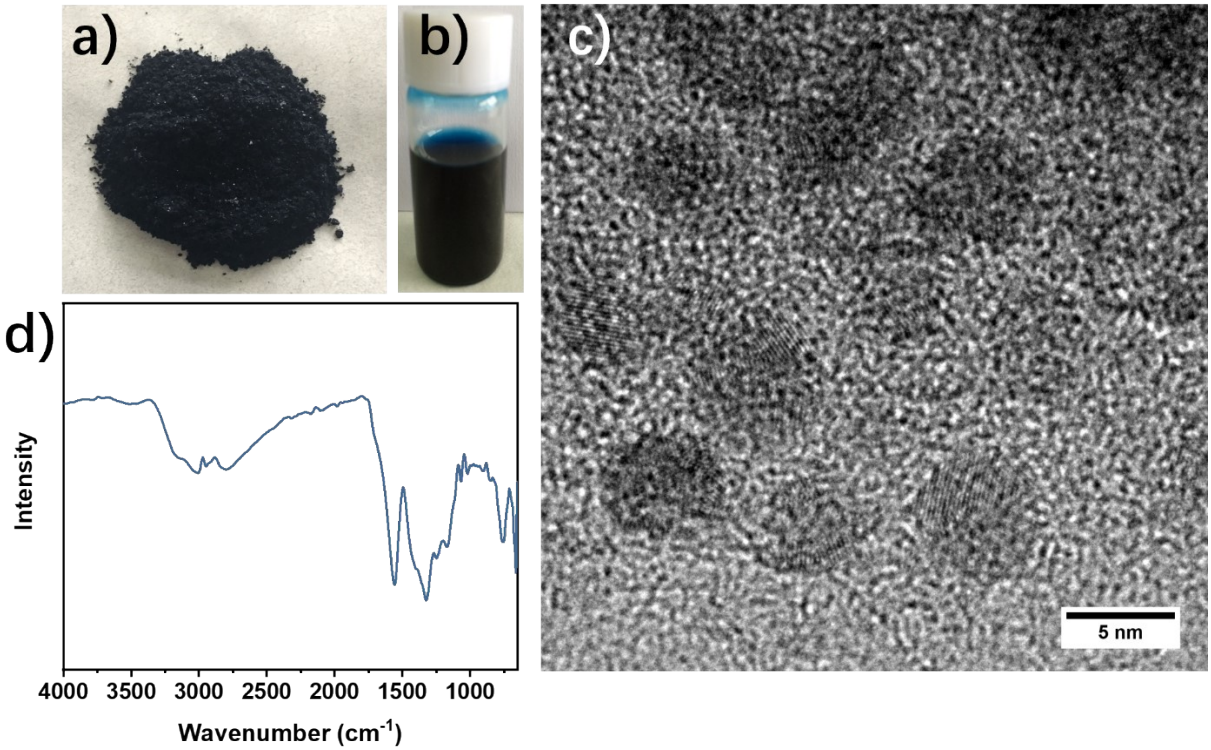

Figure S1. Digital photographs of N-GQDs (a) solid state N-GQDs, (b) aqueous solution of N-GQDs (0.72 mg mL^{-1}). (c) High-resolution TEM (HRTEM) images of N-GQDs. (d) The FTIR spectra of N-GQDs.

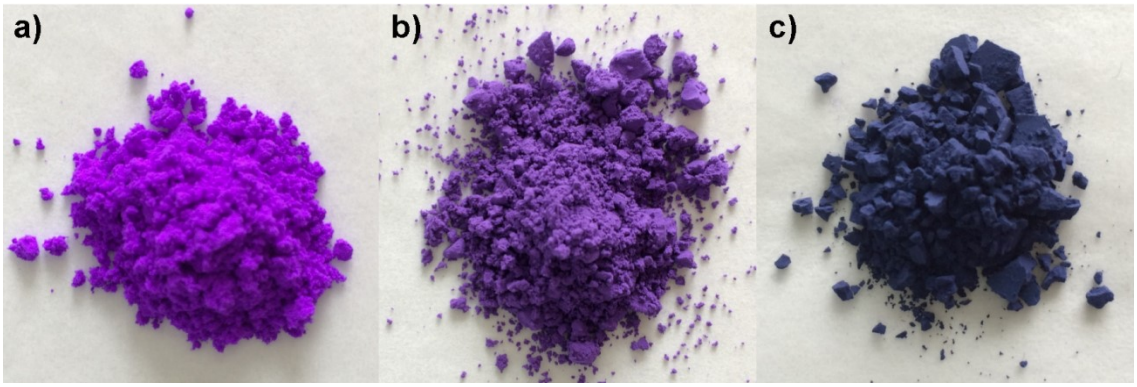

Figure S2. Digital photographs of N-GQDs@ZIF-67-*n*. (a) purple N-GQDs@ZIF-67-0, (b) violet N-GQDs@ZIF-67-50, and (c) deep blue N-GQDs@ZIF-67-150, respectively.

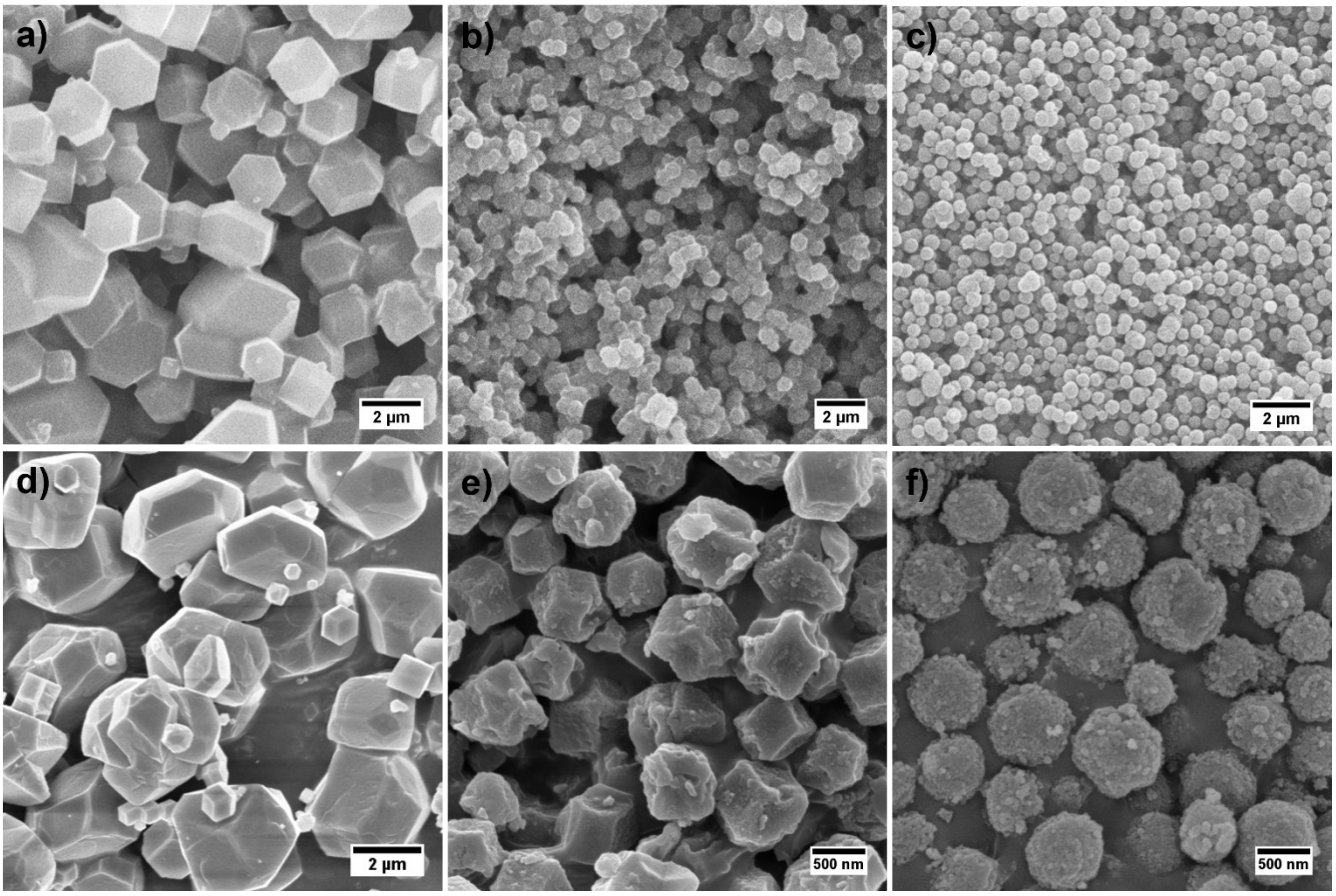

Figure S3. SEM images of (a,d) N-GQDs@ZIF-67-0, (b,e) N-GQDs@ZIF-67-50, and (c,f) N-GQDs@ZIF-67-150.

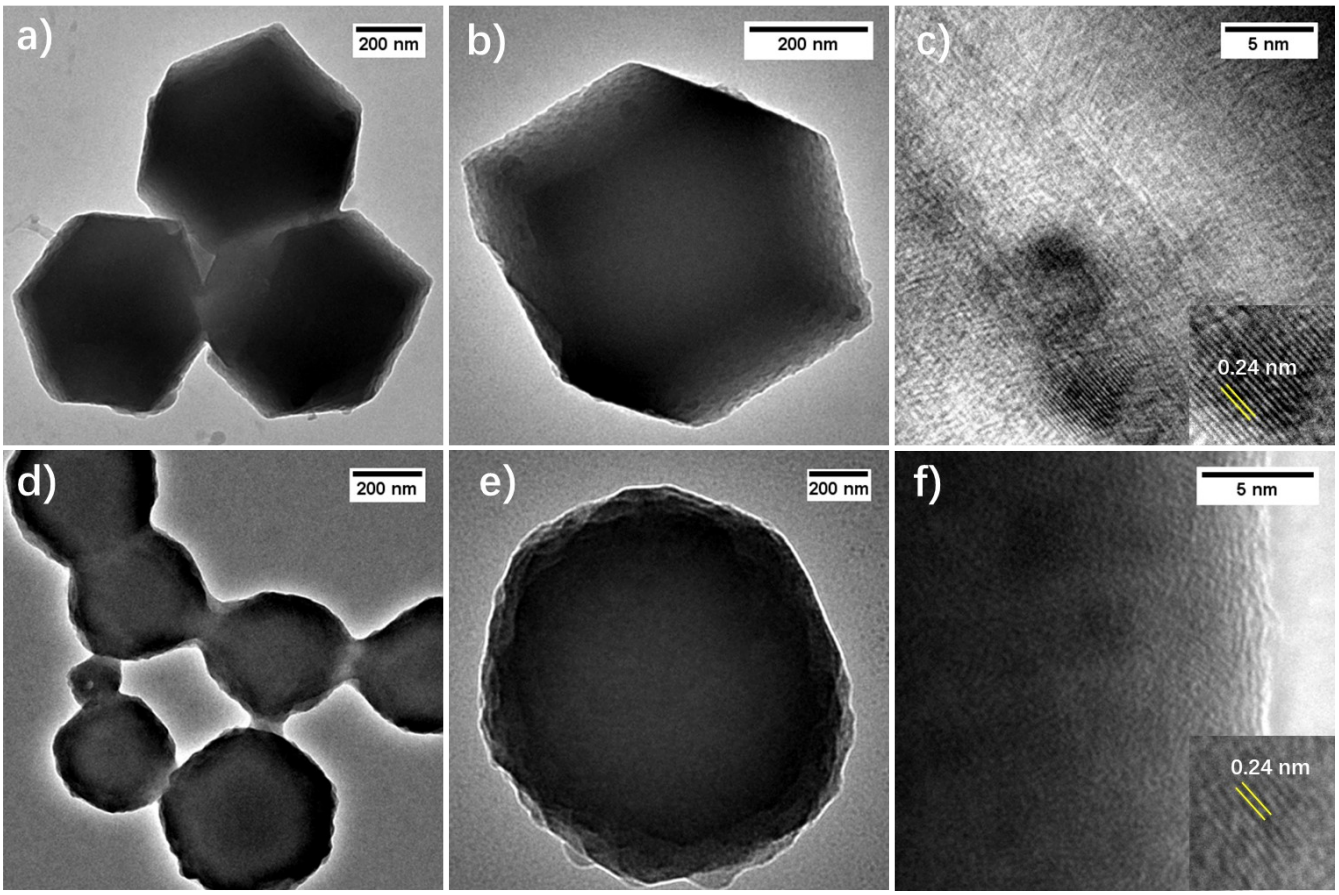

Figure S4. TEM images and HRTEM images of N-GQDs@ZIF-67-n. TEM images of N-GQDs@ZIF-67-50 (a,b), and N-GQDs@ZIF-67-150 (d,e), and HRTEM images of N-GQDs@ZIF-67-50 (c), and (f) N-GQDs@ZIF-67-150.

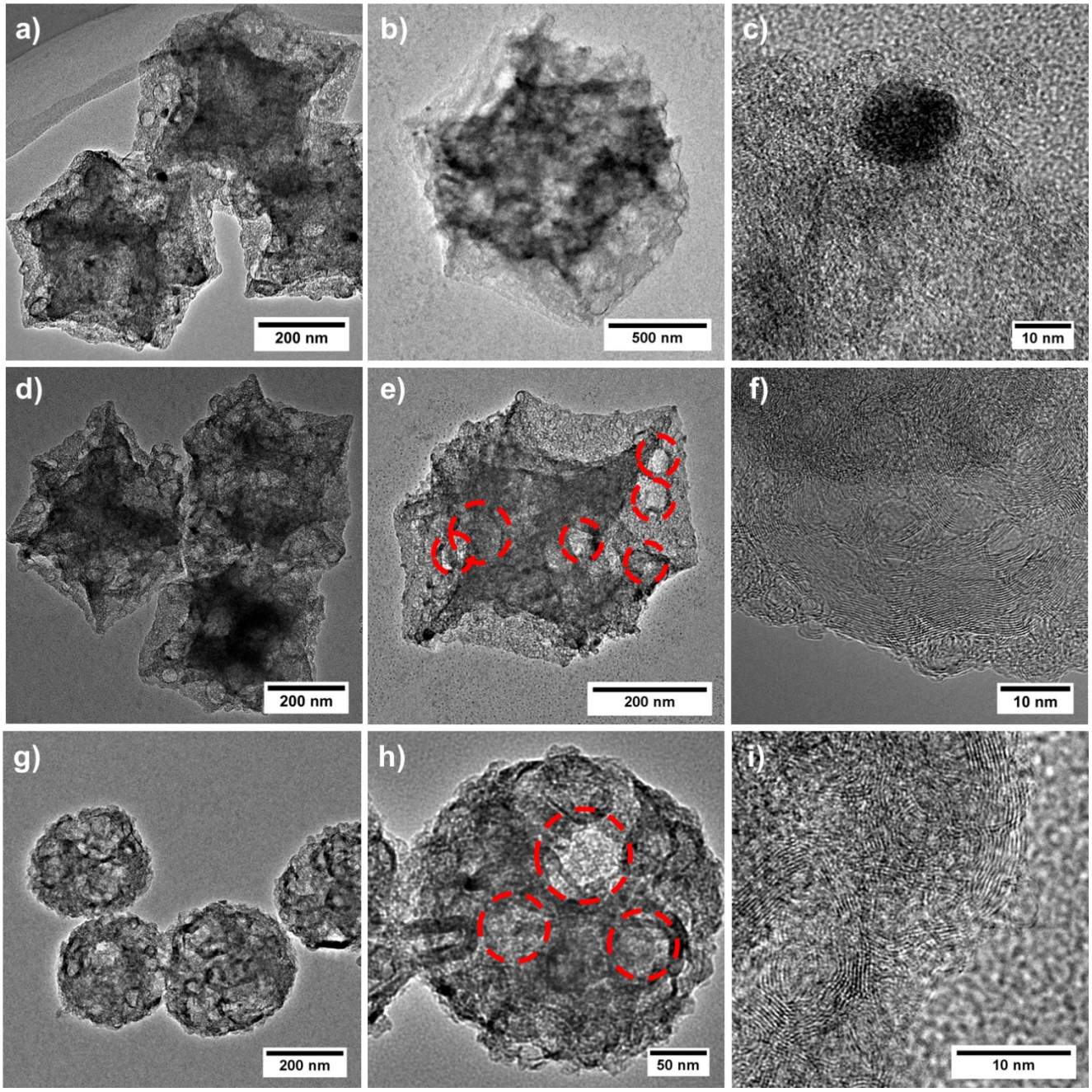

Figure S5. TEM and HRTEM images of (a-c) Co-NGC-0, (d-f) Co-NGC-50, (g-i) Co-NGC-150.

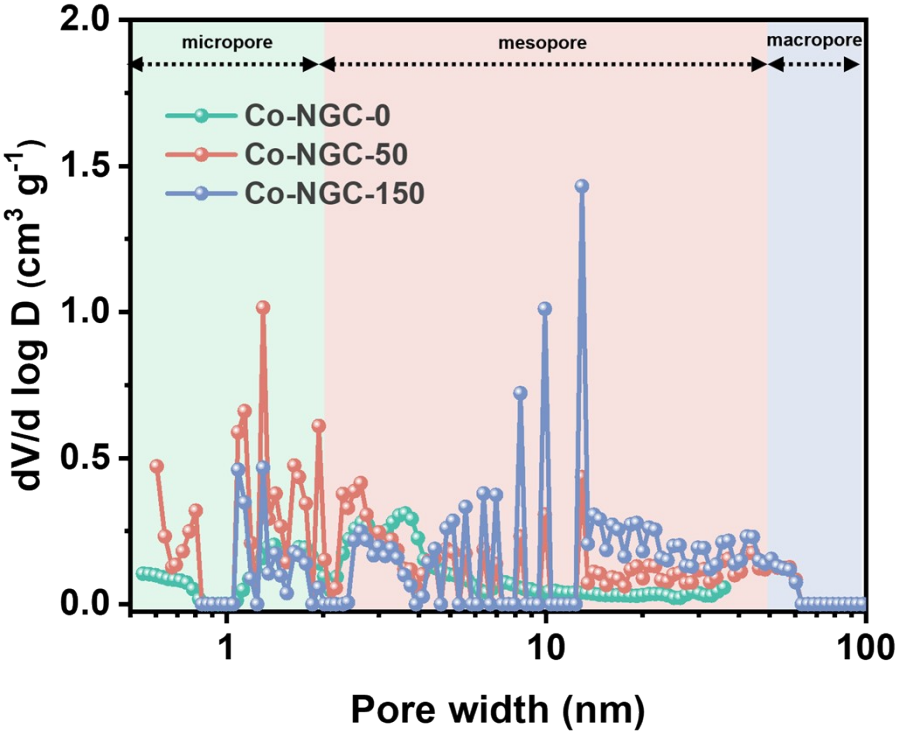

Figure S6. NLDFT pore size distribution plots of Co-NGC-*n*.

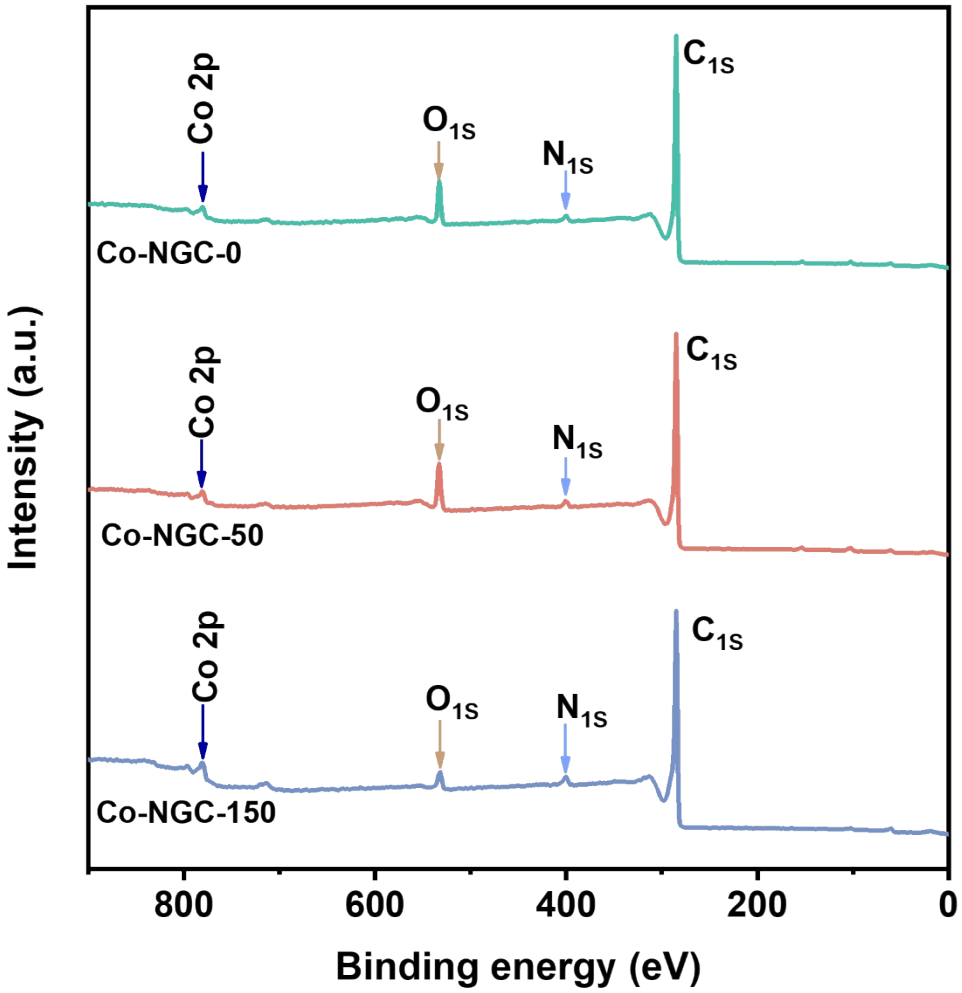

Figure S7. XPS survey spectra of Co-NGC-*n*.

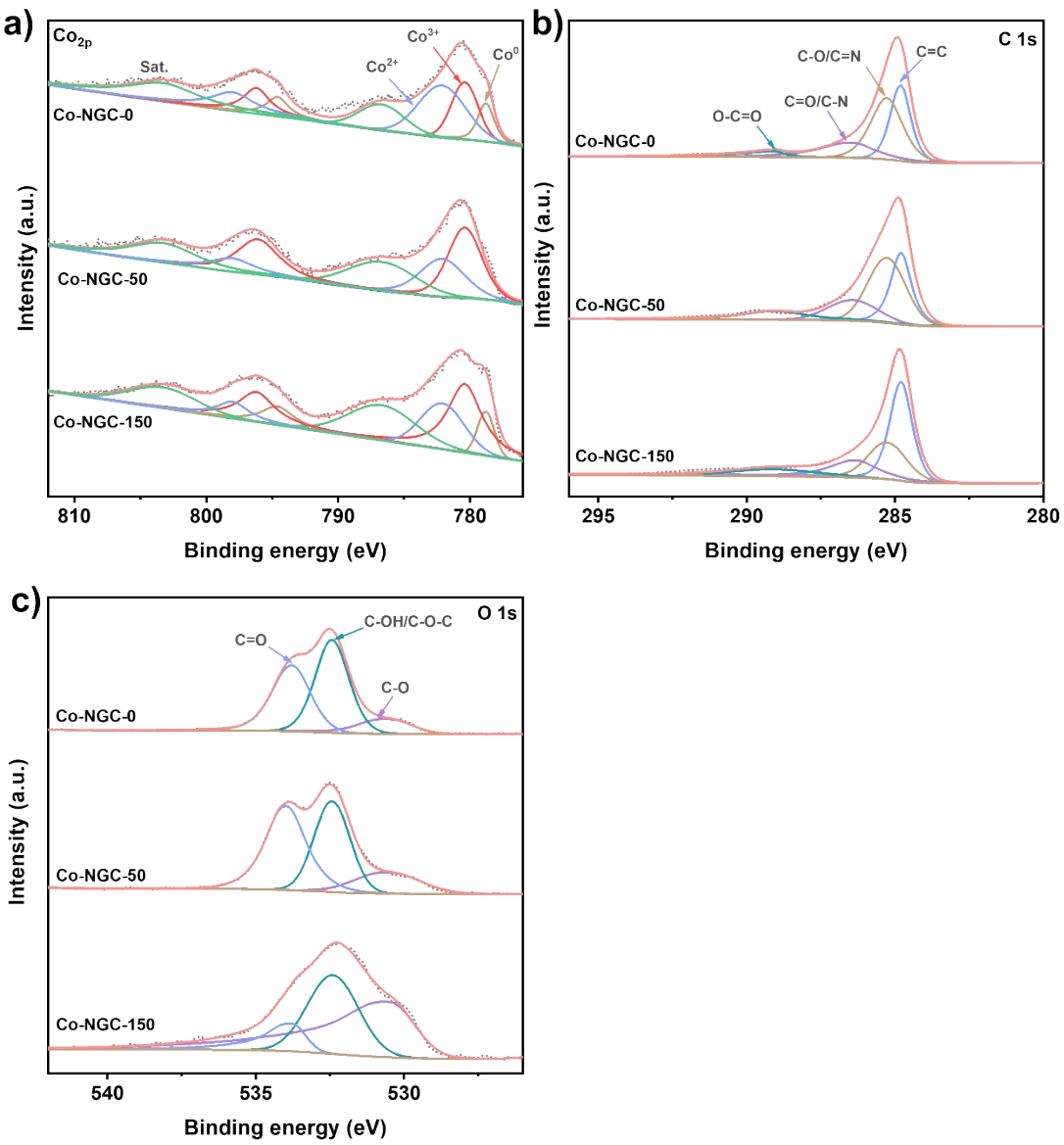

Figure S8. High-resolution deconvoluted (a) Co 2p, (b) C 1s and (c) O 1s XPS spectra of Co-NGC-*n*.

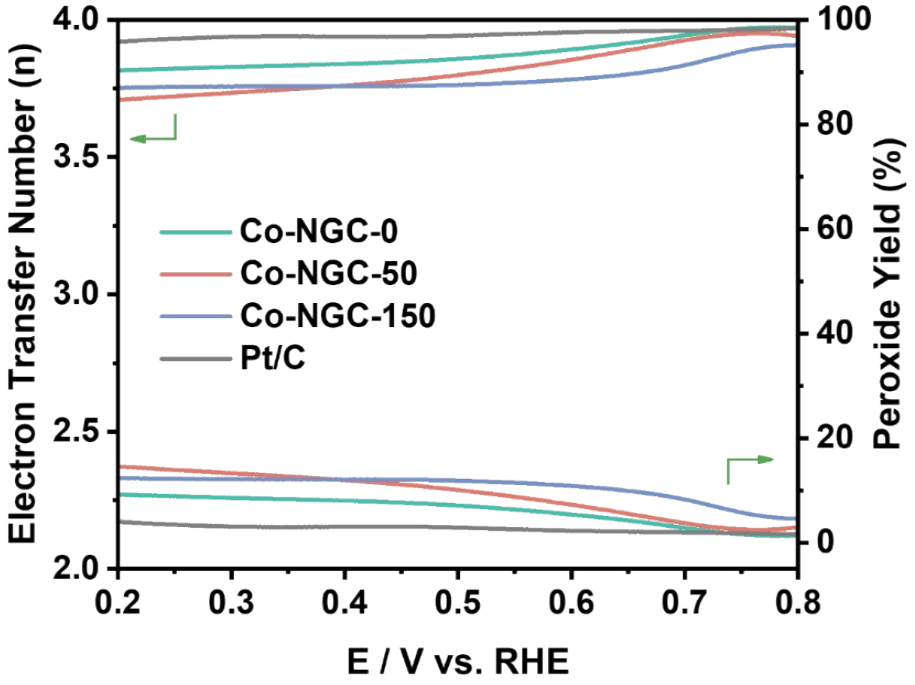

Figure S9. Electron transfer number and H_2O_2 yield.

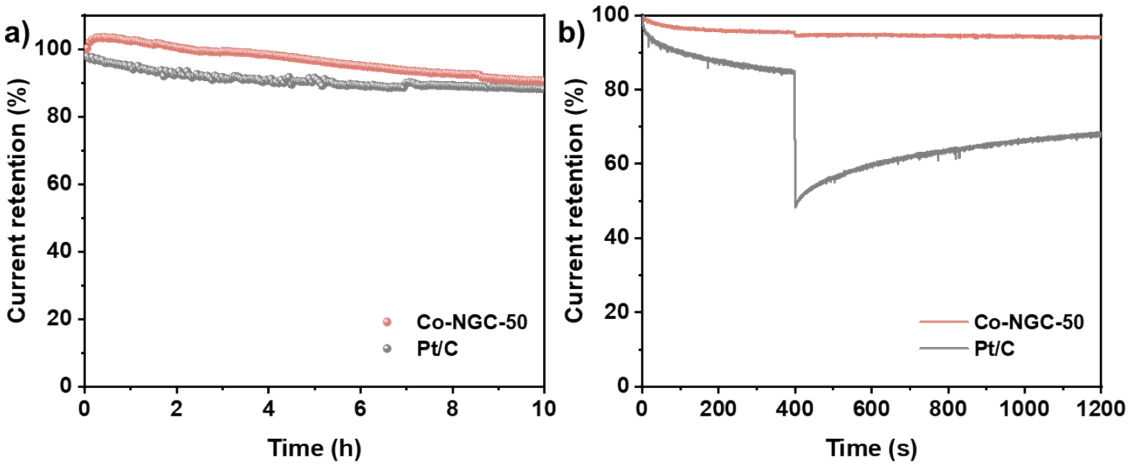

Figure S10. (a) Chronoamperometric responses of Co-NGC-50 and Pt/C in 0.1 M O_2-saturated KOH aqueous solution at 0.4 V versus RHE. (b) Chronoamperometric responses of Co-NGC-50 and Pt/C before and after the addition of methanol.

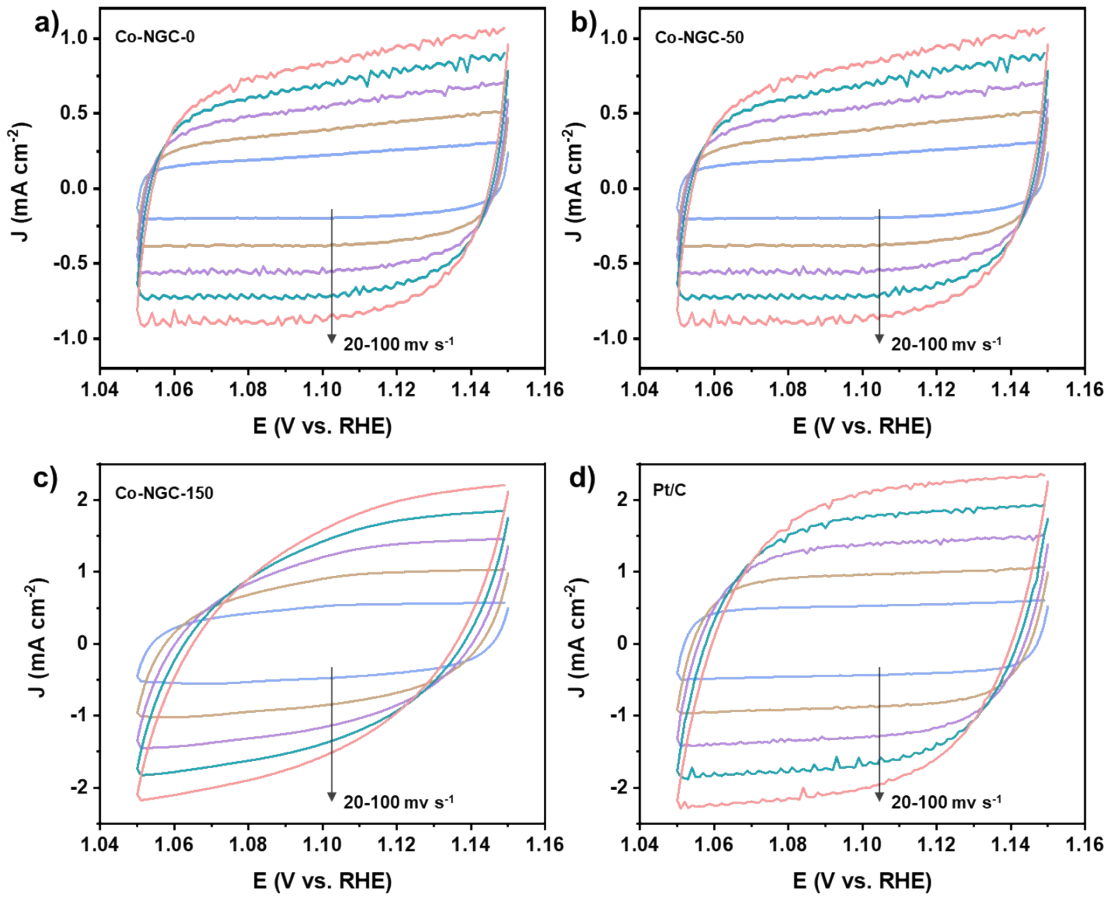

Figure S11. The cyclic voltammograms curves in the non-faradaic region at different scan rates.

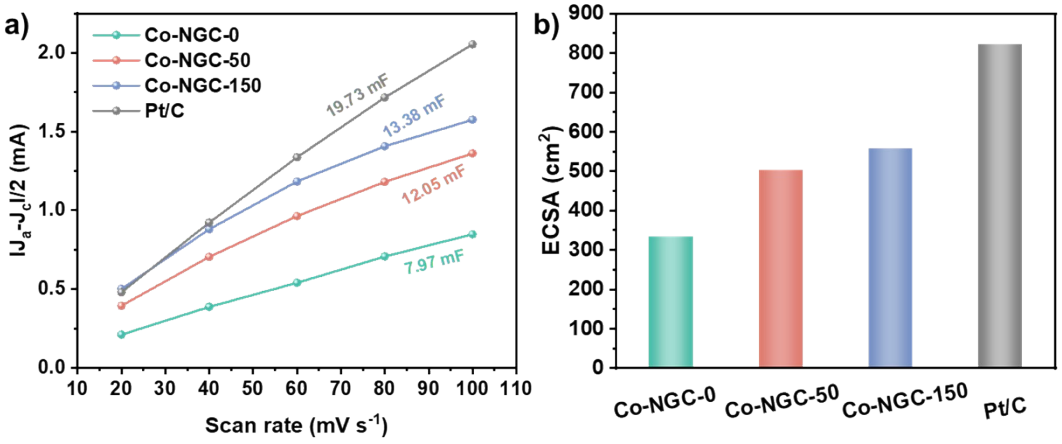

Figure S12. (a) Electrochemical double-layer capacitances (C_{dl}) of Co-NGC-*n* and Pt/C. (b) Electrochemically active surface area (ECSA) of Co-NGC-*n* and Pt/C.

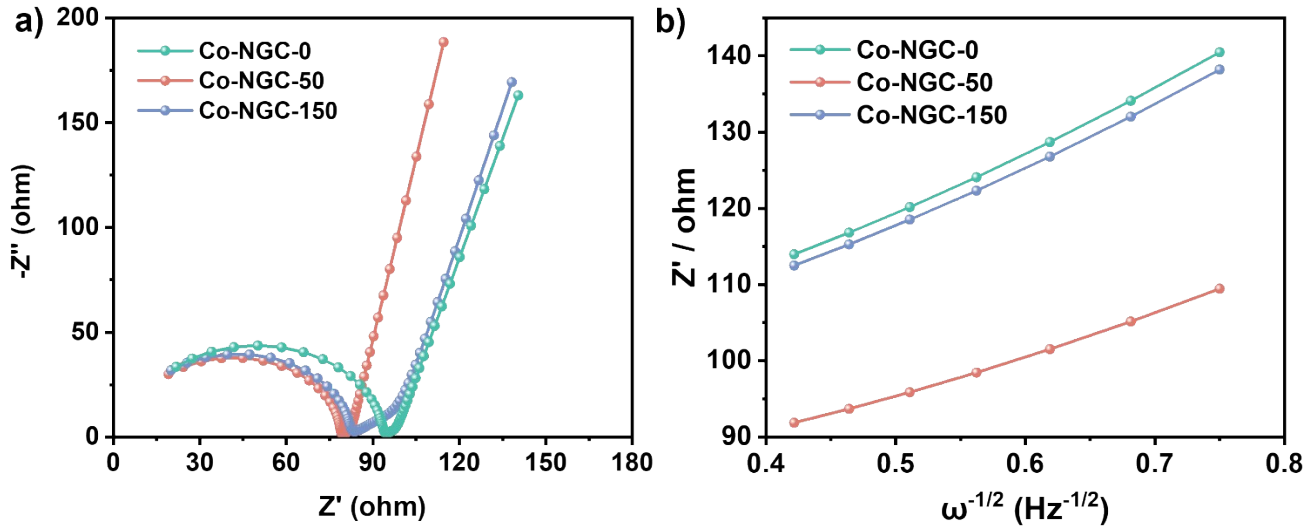

Figure S13. (a) EIS spectra at open circuit potential for Co-NGC-*n*. (b) Plot of Z′ against $\omega^{-1/2}$ based on the EIS for Co- NGC-*n*.

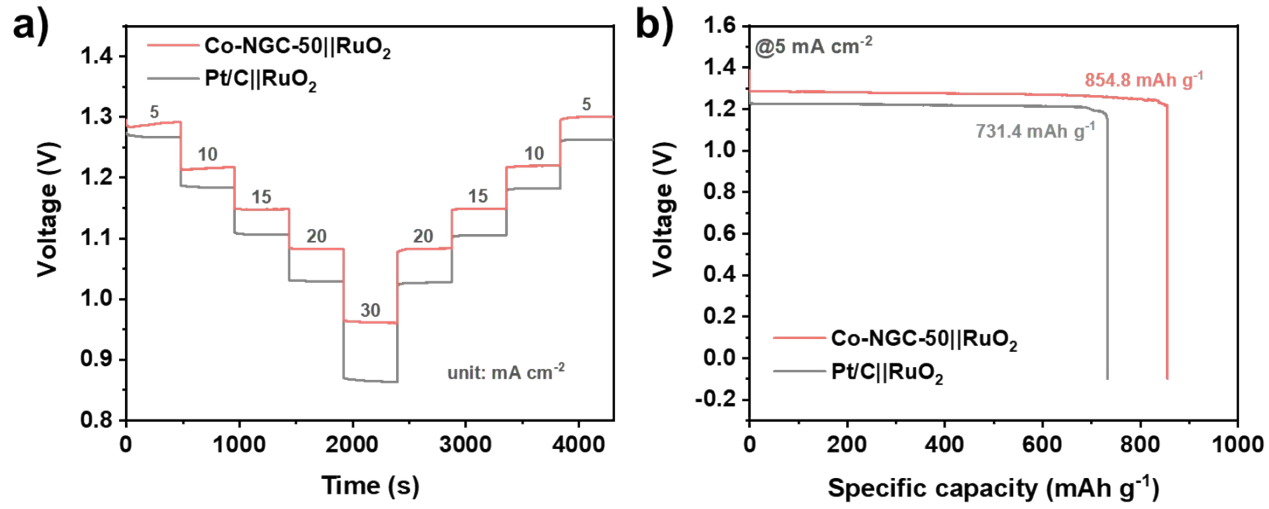

Figure S14. The liquid ZABs performance comparison between Co-NGC-50 and Pt/C catalysts. (a) Rate performance with various discharging current densities (5, 10, 15, 20, and 30 mA cm^{-2}). (b) Galvanostatic discharge curves at 5 mA cm^{-2}.

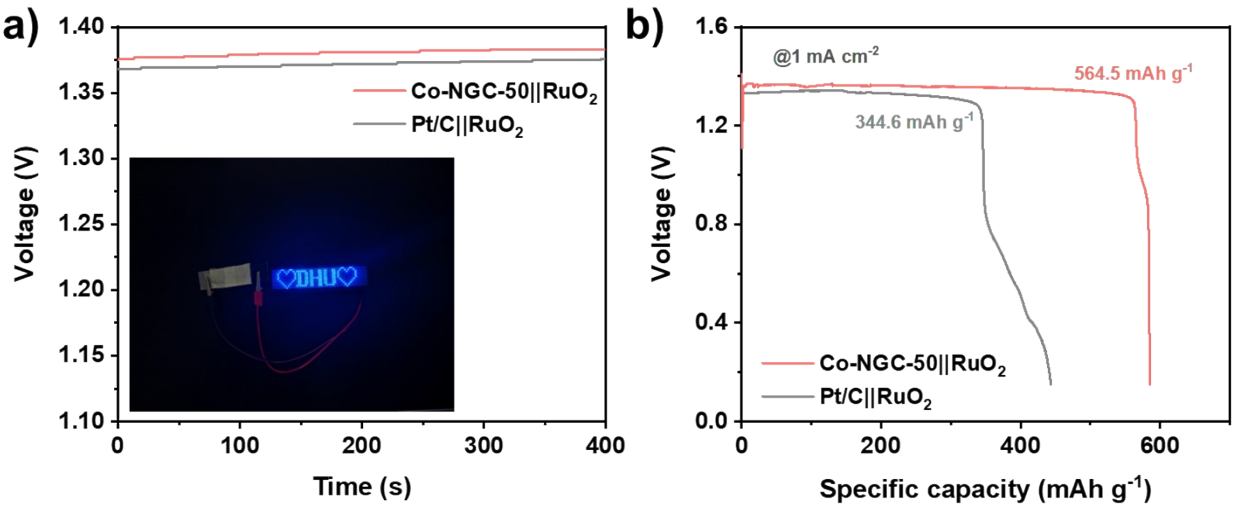

Figure S15. The flexible ZABs performance comparison between Co-NGC-50 and Pt/C catalysts. (a) The open circuit voltage plots. (b) The specific capacities at 1 mA cm^{-2}.

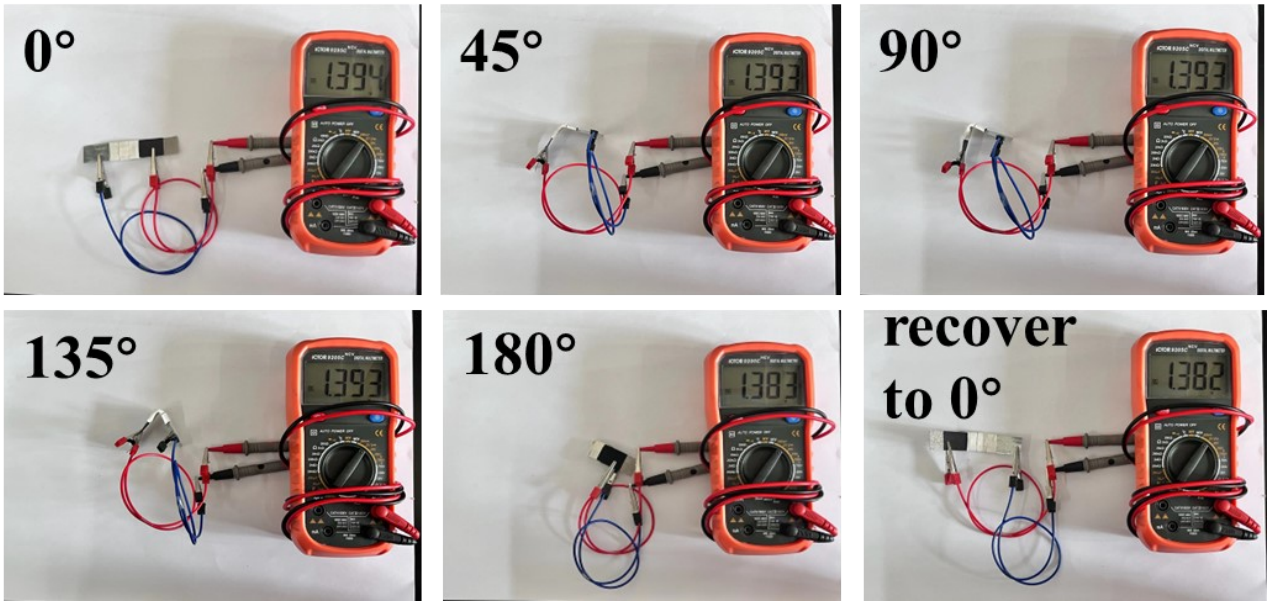

Figure S16. The open circuit voltage of the flexible ZABs equipped with Co-NGC-50 cathode under different bending angles.

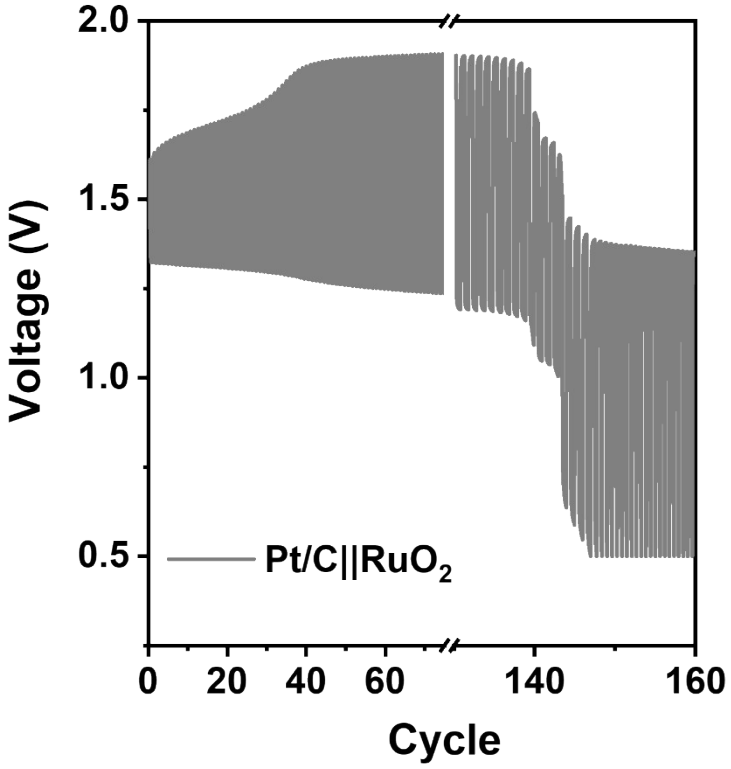

Figure S17. The cycling stability of the flexible ZABs equipped with the Pt/C || RuO_2 cathode.

Table S1. The BET specific surface areas and the total pore volumes of N-GQDs@ZIF-67-*n*.

sample	Average particle size	S_{BET} (m^2g^{-1})	V_p (cm^3g^{-1})
N-GQDs@ZIF-67-0	0.5-3 μm	1121	0.537
N-GQDs@ZIF-67-50	600 nm	1484	0.701
N-GQDs@ZIF-67-100	450 nm	1113	0.511

Table S2. Surface areas and the total pore volumes of Co-NGC-*n*.

sample	S_{BET} (m^2g^{-1})	S_{micro} (m^2g^{-1})	S_{micro}/S_{BET} (%)	V_{pore} (m^3g^{-1})	V_{micro} (m^3g^{-1})	V_{micro}/V_{pore} (%)
NGC-0	250	88	35.2	0.19	0.041	21.6
NGC-50	469	120	25.6	0.38	0.061	16.1
NGC-150	212	27	12.7	0.35	0.013	3.7

Table S3. Elemental composition of Co-NGC-n determined by XPS.

sample	N (at%)	Co (at%)	C (at%)	O (at%)
Co-NGC-0	5.22	2.85	73.05	18.88
Co-NGC-50	8.35	6.92	40.38	44.35
Co-NGC-150	20.05	15.44	44.45	20.06

Table S4. Onset potentials and /half-wave potentials and diffusion-limited currents in LSV curves for Co-NGC-*n* in O_2-saturated 0.1 M KOH solution.

sample	Onset potential *(V vs RHE)*	Half-wave potential *(V vs RHE)*	Diffusion-limited current *(mA cm^{-2})*
Co-NGC-0	0.945	0.819	-3.51
Co-NGC-50	0.975	0.835	-4.01
Co-NGC-150	0.922	0.805	-4.07
Pt/C	1.032	0.846	-5.03